Applied Catalysis A, General 612 (2021) 118011

Contents lists available at ScienceDirect

Applied Catalysis A, General

journal homepage: www.elsevier.com/locate/apcata

Lignin-based activated carbon-supported metal oxide catalysts in lactic acid production from glucose

Riikka Kupila [a,*], Katja Lappalainen [a,b], Tao Hu [b], Henrik Romar [b], Ulla Lassi [a,b]

[a] Unit of Applied Chemistry, Kokkola University Consortium Chydenius, University of Jyväskylä, P.O. Box 567, FIN-67101, Kokkola, Finland
[b] Research Unit of Sustainable Chemistry, University of Oulu, P.O. Box 4300, FIN-90014, Oulu, Finland

ARTICLE INFO

Keywords:
Heterogeneous catalyst
Lactic acid
Activated carbon
Metal oxide
Aqueous solution
Biomass

ABSTRACT

In this study, heterogeneous biomass-based activated carbon-supported metal oxide catalysts were prepared and tested for lactic acid production from glucose in aqueous solution. Activated carbons were produced from hydrolysis lignin by chemical ($ZnCl_2$) or steam activation and modified with a nitric acid treatment and Sn, Al, and Cr chlorides to obtain carbon-based metal oxide catalysts. The modification of the carbon support by nitric acid treatment together with Sn and Al oxides led to an increase in lactic acid yield. The highest lactic acid yield (42 %) was obtained after 20 min at 180 °C with the Sn/Al (5/2.5 wt.%) catalyst on steam-activated carbon treated by nitric acid. Reusability of the catalyst was also studied with the conclusion that the deposition of carbonaceous byproducts and leaching of Al oxides led to a decrease in catalyst selectivity to lactic acid.

1. Introduction

Transformation of biomass, especially non-edible and waste materials, to high-value chemicals, fuels, and materials is a promising approach for reducing dependence on fossil resources. Recently, interest among researchers in the production of lactic acid has been increasing due to its growing market demand. Lactic acid is a naturally occurring organic acid that is one of the main ingredients in the food, cosmetic, and textile industry. It is currently considered as one of the most potential feedstock monomers [1,2], that can be converted to chemicals such as pyruvic acid, acrylic acid, 1,2-propanediol, 2,3-pentanedione, lactate esters and polylactic acid (PLA) [1,3–7]. Lactic acid can be produced by chemical synthesis or by the fermentation of carbohydrates that are present in the biomass. Today, lactic acid is commercially produced mainly through the fermentation of sugars, including glucose and sucrose derived from starchy feedstocks [1,2,8–11]. However, the current fermentative production of lactic acid has several drawbacks. These include environmental and scaling-up issues arising from the raw material choices, long reaction times, waste generation as well as from the separation problems in recovering the pure lactic acid [2,9,11]. Therefore research groups have focused on novel chemocatalytic methods, which are more desirable and cost-effective, for directly converting cellulosic biomass or sugars into lactic acid or its alkyl esters [1,5,12,13].

The proposed reaction route (Scheme 1) in the conversion of cellulosic biomass-based hexoses such as glucose includes three key steps: (1) the isomerization of C_6 monomers (glucose) into fructose, (2) the retro-aldol reaction of fructose to C_3 triose intermediates, such as dihydroxyacetone, pyruvaldehyde, and glyceraldehyde, followed by (3) the conversion of trioses to lactic acid via several tandem reactions. In the reaction, two molecules of lactic acid are formed from one molecule of hexose. The main byproducts, 5-(hydroxymethyl)furfural (HMF), levulinic acid, and formic acid are also formed [14–16].

The traditional chemocatalytic methods for the conversion of biomass to lactic acid or its esters from lignocellulose through C_6 monosaccharides and C_3 trioses have been investigated over the last decade. Catalytic research with homogeneous catalysts has been focusing on the use of metal salt-based catalysts using Sn, Al, and Pb, as well as transitional metal salts, such as Zn, Ni, Fe, Co, and Cr [16–19]. Alkaline conditions have been used in the synthesis to improve the conversion and yield of lactic acid [5,17,20]. Although some of these homogeneous water-soluble salts can selectively convert glucose into lactic acid, these salts are generally expensive, highly toxic, corrosive, and/or difficult to recover afterwards [21]. Besides traditional homogeneous catalysts, solid heterogeneous catalysts are more attractive from an industrial perspective. Heterogeneous catalysts, such as Zr, Cr, Sn, Mo, W, and Pb metal oxides, as well as supported metal catalysts on zeolites and aluminum and silica oxides have been tested for the

* Corresponding author.
E-mail address: riikka.kupila@chydenius.fi (R. Kupila).

https://doi.org/10.1016/j.apcata.2021.118011
Received 2 November 2020; Received in revised form 23 December 2020; Accepted 11 January 2021
Available online 18 January 2021

conversion of trioses, sugars, and cellulose to lactic acid [10,14,22–27]. Compared to some homogenous catalysts, the lactic acid yields obtained with heterogeneous metal oxide catalysts were lower. Marianou et al. tested $SnCl_2$, SnO and Sn/γ-Al_2O_3 catalysts in glucose conversion to lactic acid with yields of ca. 33 %, 18 % and 20 %, respectively [26]. Takagi et al. used γ-AlO(OH) in the conversion of glucose to lactic acid in aqueous phase resulting yield of ca. 30 % [27]. Sn-beta-zeolites provided slightly higher yields of lactic acid. Dong et al. studied conversion of glucose with SnO_2, ZnO, Sn-Beta and Zn-Sn-Beta obtaining lactic acid yields of 6%, 12 %, 23 % and 48 %, respectively [15]. However, only a few studies on the use of activated carbon in the production of lactic acid can be found in the literature. Some studies on the oxidation of glycerol to lactic acid with carbon-supported Pt and Pd noble metal catalysts have been carried out [28,29]. Onda et al. tested the conversion of glucose to lactic acid and gluconic acid by noble metals supported on activated carbon in an alkaline, aqueous solution with the lactic acid yield of 43 % [30]. Zhang et al. used activated carbon together with metallic Zn and Ni to improve the hydrothermal conversion of glucose into lactic acid (Y = 55 %) [20]. However, high temperatures and/or alkaline conditions were used in these studies.

In catalysis, the support can play an important role, increasing the surface area and the stability of the catalyst [31,32]. The support may also improve the catalytic activity by acting as a co-catalyst and its chemical properties can be changed by specific surface functional groups and physical properties tuned by controlling the pore structures. Carbon-based support materials have been used for catalytic applications because of their properties, such as high surface areas, high thermal and chemical stability, low corrosion capability, and easy recovery from the reaction mixture [31]. Moreover, when compared to alumina and silica supports, activated carbon supports are less expensive, and the active phase can be recovered after use by burning away the carbon support [31]. As an attractive point, waste and residue biomasses can be used as a raw material in the preparation of activated carbon.

In this study, various activated carbon-based heterogeneous metal oxide catalysts were tested in the conversion of glucose to lactic acid in aqueous solution. Sn, Al, and Cr oxides were used as catalysts on activated carbon supports. The prepared activated carbon supports and catalysts were characterized by multiple techniques. As a raw material for activated carbon, hydrolysis lignin, a waste fraction from lignocellulosic biomass hydrolysis was used. The effect of the metal and the activated carbon support prepared from hydrolysis lignin by chemical or steam activation was tested in a pressurized batch system. Finally, the effect of changes in the reaction conditions (temperature, time, and pressure) on the conversion of glucose and yield of lactic acid were studied, and catalyst reusability experiments were conducted. To our knowledge, metal oxides supported on biomass-based activated carbon have now been used to convert glucose to lactic acid in aqueous solution for the first time.

2. Materials and methods

2.1. Chemicals

Hydrolysis lignin from the biomass hydrolysis process was obtained from Sekab Ab, Sweden. The following catalyst preparation materials were used: anhydrous $AlCl_3$ (99 %) from Alfa Aesar, $CrCl_3 \cdot 6H_2O$ (98 %) from VWR, $SnCl_2 \cdot 2H_2O$ (99 %) from Merck, $ZnCl_2$ (97 %) from VWR, and HNO_3 (65 %) from Merck. Anhydrous glucose (99 %) from Alfa Aesar, fructose (99 %) from Acros Organics, formic acid (>98 %) from Merck, hydroxyacetone (95 %) from Alfa Aesar, 5-(hydroxymethyl) furfural HMF (98 %) from Acros Organics, anhydrous lactic acid (98 %) from Alfa Aesar, levulinic acid (98 %) from Acros Organics, NaOH from VWR, $NaHCO_3$ (99.7 %–100.3 %) from Alfa Aesar, Na_2CO_3 (99.5 %) from Alfa Aesar, and HCl (32 %) from Merck were used as reagents and/or standard materials.

2.2. Catalyst preparation

The activated carbon support was prepared from hydrolysis lignin by chemical activation with $ZnCl_2$ or by physical activation using steam. Composition of used hydrolysis lignin is provided in Table S1 (Supplementary material). Hydrolysis lignin was dried in the oven at 105 °C and crushed to a particle size of < 0.42 mm for further use. Chemical activation was done by impregnation of the dried lignin with zinc chloride using a 2:1 mass ration of $ZnCl_2$:biomass. $ZnCl_2$ dissolved in H_2O was mixed with the biomass for 3 h at 85 °C and then dried in the oven for about 3 days at 105 °C until a constant weight was reached. The carbonization and activation of the dried $ZnCl_2$-impregnated lignin was done in a stainless steel tube in a tube furnace (Nabertherm RT200/13) at 600 °C for 2 h using a heating ramp of 10 °C min^{-1}. During the thermal heating process, the reactor was flushed continuously with inert N_2 gas (at a flow rate of 10 ml min^{-1}). Carbonization, followed by physical activation of the biomass with steam, was done in a one-step process in a stainless-steel tube in a tube furnace using a heating ramp of 10 °C min^{-1} to a temperature of 800 °C; at the target temperature steam was added by feeding water at a flow rate of 0.5 ml min^{-1} into the reactor for 2 h. During the thermal heating process, the reactor was flushed continuously with inert N_2 gas (at a flow rate of 10 ml min^{-1}). The resulting activated carbon supports were washed with hot water, dried overnight at 105 °C, and crushed and sieved to a fraction size of 0.1–0.42 mm. The supports were named AC_Z (AC zinc chloride-activated and water-washed) and AC_S (AC steam-activated and water-washed). To modify the surface, the support materials were treated with 3 mol L^{-1} HNO_3. The supports were named AC_{ZN} (AC zinc chloride-activated and HNO_3-treated) and AC_{SN} (AC steam-activated and HNO_3-treated). The treatment was performed in a round-bottom flask, with a ratio of 10:1 mass ratio of acid:support and heated for 4 h at 85 °C. After the acid treatment, the supports were filtrated and washed with hot distilled water until a constant pH was obtained, and dried in the oven at 105 °C.

Prior to the incipient wetness impregnation method, the pore

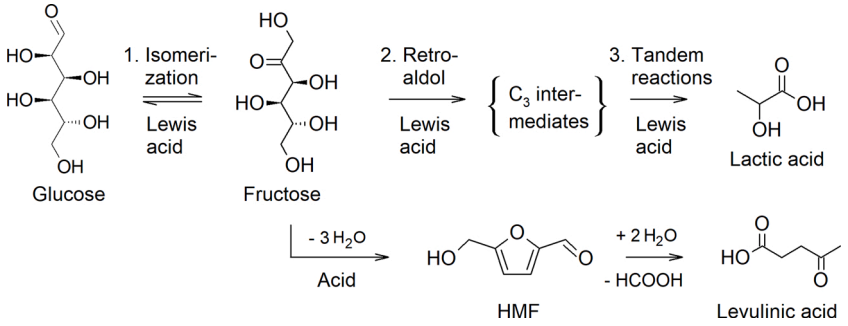

Scheme 1. Proposed reaction route for glucose conversion to lactic acid and main byproducts [14–16].

volumes of the support materials were measured by the N_2-physisorption method to calculate the volume of the impregnation solution. The amount of metal salts ($SnCl_2 \cdot 2H_2O$, $AlCl_3$, and $CrCl_3 \cdot 6H_2O$) added by impregnation on the support were calculated by assuming the targeted concentration of metal (Sn, Al, Cr) in the catalyst was 2.5–10 wt.% of the total catalyst mass. Metal salts were added in distilled water, with a drop of concentrated HCl to dissolve the precursor salts. The impregnation solution was mixed with the support, matured for 4–5 h at room temperature, and finally dried in an oven at 105 °C for 16 h. The catalysts were thermally treated in a quartz tube in a tube furnace under a nitrogen atmosphere, using a constant flush of N_2 (at a flow rate of 10 ml min^{-1}). The thermal treatment was carried out at 350 °C, using a 5 °C min^{-1} ramp and a 3 -h holding time at the target temperature. All catalysts were tested in the reaction without further reduction treatment in a hydrogen atmosphere.

2.3. Catalyst characterization

Specific surface areas (SAs) and pore size distributions were determined from the physisorption adsorption isotherms using nitrogen as the adsorbate. Determinations were performed with a Micromeritics ASAP 2020 instrument (Micromeritics Instrument, Norcross, GA, USA). Portions of each sample (0.2 g) were degassed at a low pressure (0.27 kPa) and a temperature of 140 °C for 3 h to remove the adsorbed gas. Adsorption isotherms were obtained by immersing the sample tubes in liquid N_2 (−196 °C) to achieve constant temperature conditions. Gaseous nitrogen was added to the samples in small doses, and the resulting isotherms were obtained. SAs were calculated from the adsorption isotherms according to the Brunauer–Emmett–Teller (BET) method. The precentral distribution of pore volumes (vol.%) was calculated from the individual volumes of micropores (pore diameter < 2 nm), mesopores (pore diameter 2–50 nm), and macropores (pore diameter > 50 nm) using the density functional theory (DFT) model.

The morphology of the catalyst particles was studied using a JEOL JEM-2200FS energy-filtered transmission electron microscope (EFTEM) equipped for scanning transmission electron microscopy (STEM) at the Centre for Material Analysis, University of Oulu. The STEM model is used for images, energy-dispersive X-ray spectroscopy (EDS) analysis, and quantitative mapping of the catalyst. The catalyst samples were dispersed in pure ethanol and pretreated in an ultrasonic bath for several minutes to create a microemulsion. A small drop of the microemulsion was deposited on a copper grid pre-coated with carbon (Lacey/Carbon 200 mesh copper) and evaporated in air at room temperature. The accelerating voltage in the measurements was 200 kV, while the resolution of the STEM image was 0.2 nm. The metal particle sizes were estimated visually from high-resolution STEM images of each sample.

The metal contents of the supports and catalysts were measured by ICP-OES using a Perkin Elmer Optima 5300 DV instrument. Samples weighing 0.1–0.2 g were first digested with 9 ml of HNO_3 at 200 °C for 10 min in a microwave oven (MARS, CEM Corporation). Then, 3 ml of HCl was added, and the mixture was digested at 200 °C for 10 min. Finally, 1 ml of HF was added, and the mixture was again digested at 200 °C for 10 min. Excess HF was neutralized with H_3BO_3 by heating at 170 °C for 10 min. Afterwards, the solution was diluted to 50 ml with water, and the elements were analyzed by the ICP-OES method.

The total ash content was determined by using SFS-EN 14,775 standard method.

X-ray diffractograms were recorded with the PANalytical X′Pert Pro X-ray diffraction (XRD) equipment using monochromatic $CuK_\alpha 1$ radiation (λ =1.5406 Å) at 45 kV and 40 mA. Diffractograms were collected in the 2θ range of 5°–80° at 0.017° intervals, with a scan step time of 110 s. The crystalline phases and structures were analyzed with the HighScore Plus program.

X-ray photoelectron spectroscopy analyses were performed using the Thermo Fisher Scientific ESCALAB 250Xi XPS System. The catalyst samples were placed on an indium film, with a pass energy of 20 eV and a spot size of 900 μm; the accuracy of the reported binding energies (BEs) was ±0.3 eV. Sn, Al, Zn, Cr, O, C, and N elemental data were collected for all samples. The measured data were analyzed with the Avantage V5 software. The monochromatic AlKα radiation (1486.7 eV) was operated at 20 mA and 15 kV. Charge compensation was used to determine the presented spectra, and the calibration of the BEs was performed by applying the C1s line at 284.8 eV as a reference. The approximate detection depth of the analysis was < 10 nm.

Elemental analysis of the prepared AC supports was performed by using a Flash 2000 CHN-O Organic elemental analyzer by Thermo Scientific. The ground and dried sample (about 1 mg) was placed in the analyzer and mixed with vanadium pentoxide (V_2O_5, 10 mg) to enhance the burning. The prepared sample was combusted at 960 °C for 600 s using methionine as a standard for the elements: C, H, and N, whereas the standard used for oxygen was 2,5-(bis(5-tert-butyl-2-benzoaxazol-2-yl)thiophene (BBOT).

The surface acidity and basicity of the ACs and catalysts were characterized according to the Boehm titration method [33,34]. The samples (0.1–0.2 g) were weighed and separately mixed with 50 ml of 0.01 mol L^{-1} solutions of HCl, NaOH, $NaHCO_3$, or 0.005 mol L^{-1} Na_2CO_3, and shaken for 72 h in sealed vials at room temperature. The solutions were filtered with ashless filter paper. Acidic groups were determined by the back-titration method—taking 10 ml of each filtrate, mixing with 20 ml of 0.01 mol L^{-1} HCl and finally back-titrating with 0.01 mol L^{-1} NaOH using potentiometric titration. The acidic groups on the AC were calculated [35] based on the theory that NaOH neutralizes carboxylic, lactonic, and phenolic groups and Na_2CO_3 neutralizes carboxylic and lactonic groups, while $NaHCO_3$ neutralizes only carboxylic groups. Basic sites were calculated by back-titration with 0.01 mol L^{-1}HCl; the total number of basic groups were calculated with the assumption that HCl neutralizes the basic groups on the AC surface.

Fourier Transform Infrared (FTIR) spectra were obtained using an ATR-FTIR spectrometer (Perkin Elmer Spectrum One) with diamond/ZnSe crystal. The scans were obtained in the spectral range of 4000–650 cm^{-1} with a resolution of 4 cm^{-1}, and 20 scans for each sample. Reference (blank) FTIR spectra were obtained from clean crystal.

2.4. Catalyst performance tests

For catalyst testing, HEL's manual DigiCAT pressure reactor with the hotplate and stirrer system and three parallel Mini-Range stainless steel reactors (50 mL), each with individual manometers for pressure control, was used. In a typical reaction, the catalyst was added to the reactor with 0.100 g of glucose in 20 ml of ultrapure H_2O. The reactor was purged with nitrogen and continuously mixed at 500 rpm. Heating was started after purging with nitrogen. When a reaction temperature of 180 °C was reached (in about 25 min), nitrogen was fed into the system until the desired final reaction pressure of 30 bar was attained (in about 5 min). The temperature was maintained constant through the heating of the external aluminum block in which the parallel reactors and external temperature probe were placed. After the reaction time (0–300 min), samples were collected from the reactor through the outlet vent and filtrated with a 0.45 μm (polyethersulfone) membrane filter for further product analysis. Two tests were run in parallel and the error was presented as a percentage of the average standard deviation of the two parallel tests. Recycling of the catalyst was performed after filtering the catalyst out from the reaction solution and washing it with 10 ml ethanol three times. The catalyst was then used under the same reaction conditions as in the previous cycle. Due to collection loss, the weight of the catalyst was slightly lower than the initial weight after recycling; the corresponding glucose loading was reduced to keep the weight ratio of catalyst to glucose constant.

The product analysis was performed with a Shimadzu High-Performance Liquid Chromatograph (HPLC) with a Shodex RI detector. The quantification was based on external calibration using standard solutions of glucose, fructose, lactic acid, levulinic acid, HMF, formic

acid and hydroxyacetone. The liquid samples were analyzed with a Shodex SUGAR SH1821 column (8.0 mm ID × 300 mm) with pre-column SUGAR SH-G using 5 mmol L^{-1} H_2SO_4 as a mobile phase with flow rate 1.0 ml min^{-1} and a column temperature of 40 °C. Conversion and yield were calculated from the results of the quantification by HPLC by using the following equations:

$$\text{Conversion } (\%) = \frac{C_{glucose\ initial} - C_{glucose\ at\ end\ of\ reaction}}{C_{glucose\ initial}} \quad (1)$$

$$\text{Yield } (\%) = \frac{C_{measured\ Lactic\ Acid\ in\ the\ sample}}{C_{theoretical\ max.\ of\ Lactic\ Acid\ in\ the\ sample}} \quad (2)$$

The theoretical maximum of lactic acid in the sample (Eq. 2) is calculated by assuming that 2 mol of lactic acid is obtained from 1 mol of glucose.

Compounds from product mixture were identified using Agilent 8890 GC System equipped with a mass detector (MS) and an Agilent HP5-MS Ultra Inert GC column (30 m x 0.25 mm x 0.25 mm). The oven temperature was programmed at 70 °C for 1 min, then increased to 280 °C at 10 °C min^{-1} and kept for 5 min. The injection volume was 1 ml and He flow 1 ml min^{-1}. Mass spectra were collected with an electron impact ionization of 70 eV. The Full-scan acquisition was performed with the mass detection range set at m/z 35–500. Data acquisition and analysis were executed by 5977B GC/MDS (Agilent Technologies).

3. Results and discussion

3.1. Catalyst characterization

The BET SAs, average pore diameters, and DFT pore volumes and pore distributions of the AC supports and catalysts were measured by N_2-physisorption analysis, and the results are listed in Table 1. According to the analysis, the SA and the pore volume values of chemically activated AC_Z were higher (1595 m^2 g^{-1} and 0.78 cm^3 g^{-1}) than those of steam-activated AC_S (760 m^2 g^{-1} and 0.47 cm^3 g^{-1}). After treatment with HNO_3, the SAs and pore volumes of both AC_S and AC_Z decreased about 30 %, probably due to addition of functionalities (see XPS and Boehm titration analysis) or due to the collapse of the pore walls [36–38]. However, the mesoporous volumes of both catalyst supports (AC_{ZN} and AC_{SN}) treated with HNO_3 were similar, and the main difference was in the micropore volumes; the chemically activated support AC_{ZN} had more micropores than the AC_{SN} support. The AC_{ZN} support was mainly microporous carbon, with 66 vol.% micropores and 34 vol.% mesopores. In contrast, AC_S and AC_{SN} were about 50:50 vol.% of micro:meso pores. For all supports, macropore volumes were zero. With metal impregnation, SAs and pore volumes decreased, indicating the addition of metal in the pores (Table 1). The addition seemed to occur mainly in the mesopores, since a greater decrease in their volumes was detected, though microporous volumes were also partly filled. For some catalysts, a greater decrease in porosity seemed to occur, in the following order: $Sn/Al_{5/2.5}@AC_S$ > $Sn/Al_{5/5}@AC_{ZN}$ > $Sn/Al_{5/2.5}@AC_{ZN}$ > $Sn/Cr_{5/2.5}@AC_{ZN}$ > $Sn_{10}@AC_{ZN}$ > $Sn/Al_{5/2.5}@AC_{SN}$.

Metal contents of the supports and catalysts were measured by total ash content analysis and by ICP-OES. Results of the ash analysis and ICP-OES analysis from activated carbon supports AC_Z, AC_{ZN}, AC_S, and AC_{SN} are presented in Table S2 (Supplementary material). Without acid treatment, the chemically activated AC_Z support contained about 5 wt.% of zinc (Table S2) and total metal content was 7.6 wt.% by ash analysis. After AC_Z was treated with HNO_3, zinc metal was removed from the support and ash content decreased to zero. The steam-activated support AC_S contained 0.5 wt.% of Ca and Na; other metals, such as Fe, Mn, Mg, K, and Zn were present at less than 0.1 wt.% and total ash content was 2.3 wt.%. After acid treatment, total residual metal content was less than 0.3 wt.% for both AC_{ZN} and AC_{SN}.

The active metal contents of the catalysts Sn, Al, and Cr were measured by ICP-OES analysis. The results are presented in Table 1. From the ICP-OES analysis, determined Sn and Al contents were close to the targeted ones. Slightly lower amounts of Sn and Al were detected from the non-acid-treated catalyst $Sn/Al_{5/2.5}@AC_S$. In some cases, acid treatment and the presence of oxygen functionalities (see XPS and Boehm-titration) on the surface has been claimed to be important, by making the surface more accessible for metal precursors at the catalyst preparation and impregnation step—i.e., acting as anchoring sites for the metal precursors on the surface—or by making the surface more hydrophilic, so that the metal precursors can adsorb to the internal surface of the pores [31,39,40].

The morphology of the catalyst particles was studied with an EFTEM/STEM microscope. The STEM mode was used for images and combined with EDS analysis and quantitative mapping to detect the elemental composition of the materials. The STEM-high angle annular dark field (STEM-HAADF) image of the $Sn/Al_{5/2.5}@AC_{SN}$ catalyst and the quantitative mapping presented in Fig. 1 show an equal distribution of aluminum and tin on the surface of the AC. The STEM-HAADF images from all the supports and catalysts are presented in Fig. S1 and Fig. S2 (Supplementary material). From the images of the supports, large particles of zinc oxide are seen on AC_Z (Fig. S1 c), which disappear from AC_{ZN} after acid treatment (Fig. S1 d). From the catalyst images (Fig. S2), the particle sizes on the surfaces were estimated to be less than 10 nm, with a particle size of approximately 3–5 nm; some aggregations were also detected from the surfaces (~ 20 nm). The N_2-physisorption analysis indicated that mainly mesopores and some of the micropores were filled by impregnation of the catalyst particles on the support. The STEM

Table 1
N_2-physisorption analysis of the ACs and catalysts. Intended active metal contents and measured metal contents of the ACs and catalysts by ICP-OES analysis.

Sample *	Physisorption BET		DFT			Targeted metal content [wt.%]			Metal content by ICP-OES [wt.%]		
	BET SA [m^2 g^{-1}]	Aver pore diam [nm]	Total volume [cm^3 g^{-1}]	Meso-pores [cm^3 g^{-1}]	Micro-pores [cm^3 g^{-1}]	Sn	Al	Cr	Sn	Al	Cr
AC_Z	1595	2.3	0.78	0.33	0.45	–	–	–	0	0	0
AC_{ZN}	1090	2.1	0.50	0.17	0.33	–	–	–	0	0	0
$Sn_{10}@AC_{ZN}$	855	2.0	0.37	0.10	0.27	10.0	–	–	9.2	0	0
$Sn/Al_{5/5}@AC_{ZN}$	505	1.8	0.19	0.02	0.17	5.0	5.0	–	4.9	5.0	0
$Sn/Al_{5/2.5}@AC_{ZN}$	720	1.9	0.29	0.06	0.22	5.0	2.5	–	5.1	2.6	0
$Sn/Cr_{5/2.5}@AC_{ZN}$	875	1.9	0.36	0.10	0.27	5.0	–	2.5	5.0	0	2.3
AC_S	760	2.9	0.47	0.26	0.21	–	–	–	0	0	0
AC_{SN}	553	2.7	0.32	0.16	0.16	–	–	–	0	0	0
$Sn/Al_{5/2.5}@AC_S$	355	2.5	0.18	0.08	0.11	5.0	2.5	–	4.3	2.3	0
$Sn/Al_{5/2.5}@AC_{SN}$	539	2.1	0.24	0.07	0.17	5.0	2.5	–	4.7	2.9	0

* Z = chemical act., S = steam act., N = HNO_3 treat.

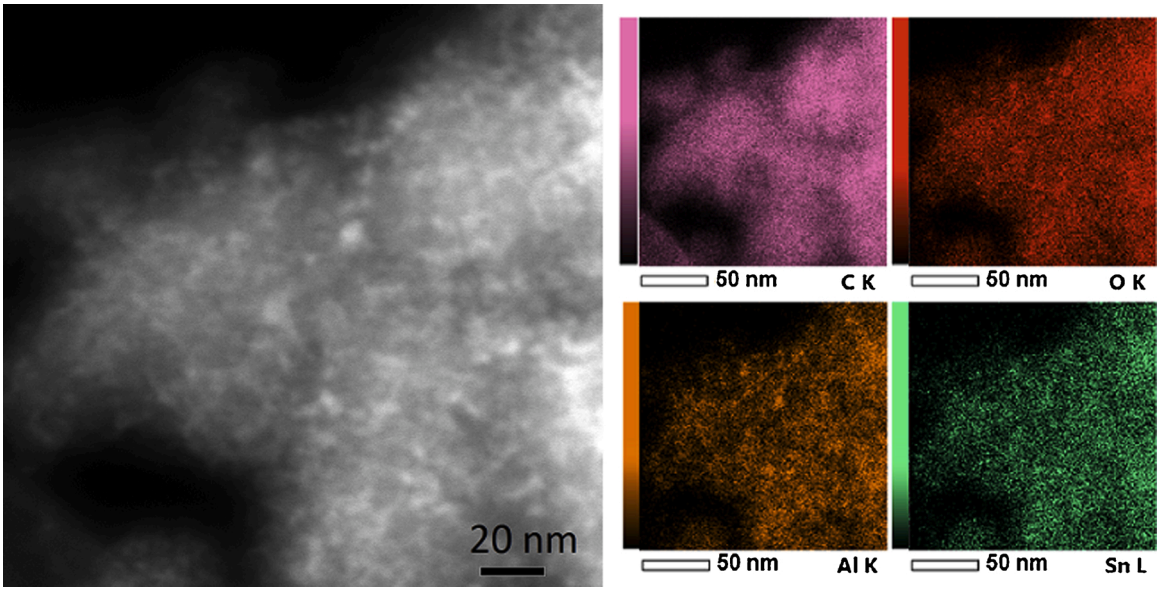

Fig. 1. STEM-HAADF image and quantitative mapping from the $Sn/Al_{5/2.5}@AC_{SN}$ catalyst.

images verified that small nanoparticles were able to enter into the support pores. However, some of the smallest pores can be blocked by the particles at the pore entrance. Especially for the catalysts $Sn/Al_{5/5}@AC_{ZN}$ and $Sn/Al_{5/2.5}@AC_{ZN}$ (Figs. S2 b and c), there appeared to be some aggregations, which could be due to an accumulation of nanoparticles in the pores. These could be the reason for the larger decrease in the BET SA and pore volumes. Overall, the particles seemed to be distributed uniformly on surfaces with small particle sizes.

XRD analysis was performed to verify the metal phases of the catalysts. The diffraction patterns are presented in Fig. S3 (Supplementary material). For all supports and catalysts, broad peaks at 23.8° and 44.2° were detected, representing amorphous carbon. For AC_Z support, peaks at 31.7°, 34.3°, 36.1°, 47.4°, 56.5°, 62.7°, 67.8°, and 68.9°, representing ZnO (JCPDS file No. 04-003-2106) were detected, which disappeared after acid treatment (see Fig. S3 a, XRD pattern of AC_Z and AC_{ZN}). For Sn-catalysts (Fig. S3 b), the oxidized metal phase of tin(IV)oxide (SnO_2) (JCPDS file No. 00-001-0657) was detected, though the peaks representing SnO_2, at around 26.3°, 33.5°, 51.7°, and 64.2°, were rather small for bi-metal catalysts. For Al and Cr, no clear peaks could be detected, probably because of the small particle size or a low concentration of the catalyst material. Overall, diffractograms presented no high crystallinity for Sn, Al, or Cr, indicating the presence of amorphous phases and/or very small particles on the surface of the support, which were also seen on the STEM images.

The metal phases of the catalysts were confirmed with XPS (Fig. S4 and Table S3, Supplementary material). According to the analysis, metal oxides with peaks at 487.2 eV and 495.6 eV (Fig. S4 a) corresponded to $Sn3d_{5/2}$ and $Sn3d_{3/2}$ [25], respectively, representing tin(IV) oxide (SnO_2), and with peaks at 74.5 eV (Fig. S4 b) corresponded to Al2p oxide, most likely representing AlO(OH) [41], were detected from the spectrums of catalysts containing Sn and Al on support AC_S, AC_{SN}, and AC_{ZN}. The XPS spectrum peaks of the Sn/Cr catalyst on AC_{ZN} (Figs. S4 a and c) at 487.2 eV and 495.6 eV corresponded to $Sn3d_{5/2}$ and $Sn3d_{3/2}$, respectively, representing SnO_2, and peaks at 577.4 eV and 586.9 eV corresponded to $Cr2p_{3/2}$ and $Cr2p_{1/2}$ [42], respectively, representing Cr_2O_3. The support AC_Z spectrum (Fig. S4 d) peaks at 1045.7 eV and 1022.6 eV corresponded to $Zn2p_{1/2}$ and $Zn2p_{3/2}$, respectively, representing ZnO [43].

3.1.1. Surface functionality

The surfaces of the AC supports were analyzed with XPS, FTIR and Boehm titration for information about their content and functionality. The elemental analysis (C,H,*N*,O) of the support material was compared to the total carbon, oxygen and nitrogen content obtained by XPS; however, elemental analysis analyses the total bulk material, while XPS analyses only the uppermost layer. Examples of the C1s and O1s spectra from the XPS analysis are presented in Fig. S5 (Supplementary material). The peaks from the C1s spectra indicated that most of the carbon was present as graphitic conjugated carbon (at 284.8 eV) and non-conjugated carbon (at ~285 eV). Also, carbon-oxygen type functionalities were present at 286.6 eV (from phenolic, alcoholic, or etheric functional groups) and at 288.8 eV (from carboxylic, anhydride, ester, or lactone groups) [44–47] (Table S3, Supplementary material). The highest total carbon content, detected by both XPS and elemental analysis, was in steam-activated AC_S and it decreased after the chemical treatments due to the addition of heteroatoms (Table 2). The more drastic decrease in the total carbon content, detected by XPS rather than by elemental analysis, indicated that the functional groups were attached to the surface. The XPS O1s analysis of the chemically activated AC_Z showed a higher total oxygen content than that of AC_S, most likely due to oxygen atoms bound to Zn as ZnO [48], which were present from the preparation step. When activated carbon was treated with nitric acid, the total oxygen content of the AC_{SN} was three times higher than on the surface of the plain steam-activated catalyst support (AC_S) (Table 2). The nitric acid treated support AC_{ZN} showed a higher content of total oxygen than AC_Z and four times higher than AC_S. Similarly, confirmed by elemental analysis, the oxygen content of the HNO_3 treated supports was about four times higher than of the untreated ones and was highest in the AC_{ZN} support. The increase of oxygen functionalities after HNO_3 treatment was detected mainly as oxygen functionalities from the O1s scan at 532.3 eV (Table S3, Supplementary material), which can be identified as carbonyl oxygen from functionalities such as lactone, ester, carboxylic or anhydride, and oxygen atoms from phenol or ether groups. However, the identification is not clear since the same functionality can give a signal at different BEs, and it also depends on the fittings of the peaks [44,45,47,49–51]. It has been reported that oxidation by nitric acid treatment increases the oxygen content on the activated carbon, and especially the number of acidic functionalities such as carboxyl groups [36,38,51,52]. A small increase in the nitrogen content was also detected on ACs after nitric acid treatment. The nitric acid oxidation is also known to result in a number of nitro groups via the nitration mechanism of aromatic ring [53]. This was indicated by the FTIR spectrum of AC_{ZN} (Fig. S6 a, Supplementary material).

The acidic and basic group concentration of the supports was studied

Table 2
The elemental analysis of the bulk material, and surface analysis according to the XPS and Boehm titration of the AC supports.

Sample *	Elemental analysis				XPS			Boehm titration	
	Total C [%]	Total O [%]	Total N [%]	Total H [%]	Total C [%]	Total O [%]	Total N [%]	Total acidic groups [mmol g^{-1}]	Total basic groups [mmol g^{-1}]
AC_S	90.1	2.7	0.4	0.6	91.3	8.3	0.4	0.2	0.4
AC_{SN}	78.2	10.7	1.1	0.4	68.8	29.4	1.8	1.2	0.0
AC_Z	79.1	6.2	0.8	0.8	62.2	26.6	0.7	0.7	0.0
AC_{ZN}	66.9	21.1	2.8	0.8	59.1	38.2	2.5	2.7	0.0

* S = steam act., Z = chemical act., N = HNO_3 treat.

with the Boehm titration method (Table 2). The titration indicated that only minor amounts of acidic functionalities and some basic functionalities (e.g., chromene or pyrone [31]) were present on AC_S. The explanation in the literature is that the high temperatures (800 °C) used for steam activation can destroy most of the functional groups on the surface of AC [51], seen also from the FTIR spectrum (Fig. S6 a). A slightly higher total acidic group concentration was observed on chemically activated AC_Z as compared to the steam-activated AC_S. This could be due to the lower temperature (600 °C) used in the preparation of AC_Z, leaving more functional groups on the surface, or from the presence of ZnO. According to the Boehm method (Table 2), after nitric acid treatment, a higher content of total acidic groups, at 1.2 mmol g^{-1} and 2.7 mmol g^{-1} were detected on AC_{SN} and AC_{ZN}, respectively, than on untreated AC_S and AC_Z, due to an increase in carboxylic, lactonic, and phenolic groups (Fig. S7, Supplementary material). This was in good agreement with the results from the XPS analysis. No basic groups were detected on the AC_Z, AC_{ZN}, or AC_{SN} surfaces with Boehm titration.

After the addition of metals to the supports, the total carbon content decreased, while the oxygen content increased, most likely due to the addition of metal oxides or hydroxides, which can be seen from the metal-oxygen bonds at 531.2 eV or 532.3 eV [54–56] (Table S3, Supplementary material) according to the XPS analysis. A decrease in nitrogen content was also noted after the addition of metal (Table S3), indicating that nitrate/nitro groups introduced to the surface during oxidation with nitric acid decreased after catalyst preparation, since the nitro groups begin to decompose at about 270 °C [53]. Boehm titration analysis was conducted for the catalysts by back-titrating with NaOH to determinate their total acidic group concentration. Besides the acidic groups (carboxylic, lactonic, and phenolic) on the aromatic carbon framework, inorganic components such as metal hydroxides may take up protons and/or precipitate during the acidification step in the Boehm titration procedure, thereby affecting the total acidity of the sample [57]. The total acidity increased after the addition of metal oxides to AC_S and AC_{SN}, and was 1.1 mmol g^{-1} and 1.7 mmol g^{-1} for $Sn/Al_{5/2.5}@AC_S$ and $Sn/Al_{5/2.5}@AC_{SN}$, respectively. This is most likely due to oxidized metals or acidic species created during the metal impregnation on AC, seen also as an increase in O1s XPS analysis at 532.3 eV, indicating an increase in metal-oxygen bonds or carbon-oxygen bonds (Table S3, Supplementary material). On the other hand, for the catalysts impregnated on AC_{ZN}, the total acidity did not change after the addition of metals and was about 2.6 mmol g^{-1} for $Sn_{10}@AC_{ZN}$, $Sn/Al_{5/2.5}@AC_{ZN}$ and $Sn/Cr_{5/2.5}@AC_{ZN}$. Further investigations using Boehm titrations were performed for the heat-treated ACs. Heat treatment was performed in a similar manner as for the catalysts—at 350 °C for 3 h under N_2. As a result, the total acidity decreased by about 20 %, and mainly the carboxylic groups seemed to break down (Fig. S7, Supplementary material); these are groups that break easily at lower temperatures [44,51]. This could be why the total acidity did not increase with the addition of metal oxides on the AC_{ZN} support—it contained more carboxylic groups, which could have decomposed in the heat treatment process during the catalyst preparation. Presence of carbonyl groups after catalyst preparation and heat treatment on carbon was verified from the FTIR spectrum (Fig. S6 b), however, peaks indicating the presence of nitro groups were absent. This was in agreement with the XPS and titration analyses.

3.2. Catalytic studies

3.2.1. Preliminary studies

Preliminary studies with chlorides of Sn, Al, and Cr, and chlorides of Sn + Al, Al + Cr, and Sn + Cr metal combinations were done to study the conversion of glucose to lactic acid under the following conditions: 2 h at 180 °C, 30 bar, and 500 rpm, using 0.100 g of glucose in 20 ml of H_2O. $SnCl_2*2H_2O$, $AlCl_3$, or $CrCl_3*6H_2O$ were used as single catalysts at a concentration of 0.1 mmol, and at concentrations of 0.05 mmol each metal in combination. The reaction parameters and catalyst amounts were adapted from Deng et al. [16]. Results from the test are shown in Fig. 2. For all the homogeneous metal salts tested, except $SnCl_2$, 100 % conversion of glucose was obtained. The lactic acid yield of the single Sn catalyst was low (7%). Single Cr and Al catalysts had higher lactic acid yields (~20 %); however, levulinic acid was produced in an almost 1:1 ratio with lactic acid. The lactic acid yield from the Al + Cr combination was about the same as that from single Al and Cr catalysts, though a lower amount of levulinic acid was produced. The highest lactic acid yields, 37 % and 36 %, were obtained from the Sn + Cr and Sn + Al combinations, respectively. Based on the preliminary study results, the best working metal combinations (tin combined with aluminum or chromium) were selected as heterogeneous catalysts on activated carbon for further analyses of lactic acid production.

3.2.2. Effect of the metal oxide on supported AC catalyst

The conversion of glucose (0.100 g) by heterogeneous metal catalysts supported on activated carbon was studied at 180 °C, 500 rpm, 30 bar with 0.100 g of the catalyst in 20 ml of H_2O (Fig. 3). The effect of the metal was studied using a carbon-supported tin oxide catalyst as well as tin oxide combined with oxides of aluminum or chromium on the carbon support. Furthermore, the ratio of the metals in the catalysts was modified. Chemically activated and nitric acid-treated activated carbon (AC_{ZN}) was used as support. AC_{ZN} treated in a manner similar to the catalysts, in a N_2 atmosphere at 350 °C for 3 h, was used as a reference

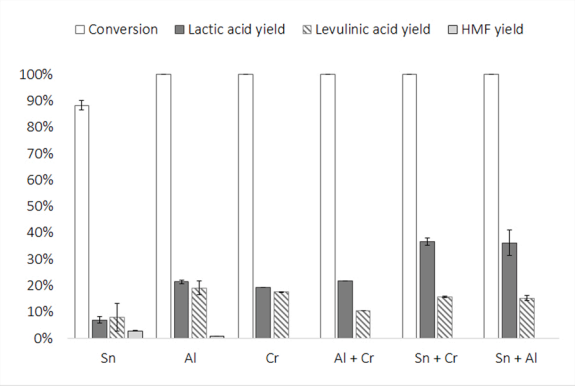

Fig. 2. Glucose conversion and product yields at 180 °C, 30 bar, 500 rpm, 120 min, with 0.1 g of glucose in 20 mL H_2O and 0.1 mmol of catalyst ($SnCl_2*2H_2O$, $AlCl_3$, and $CrCl_3*6H_2O$). For dual catalyst combinations (Al + Cr, Sn + Cr, Sn + Al), 0.05 + 0.05 mmol of catalyst load was used.

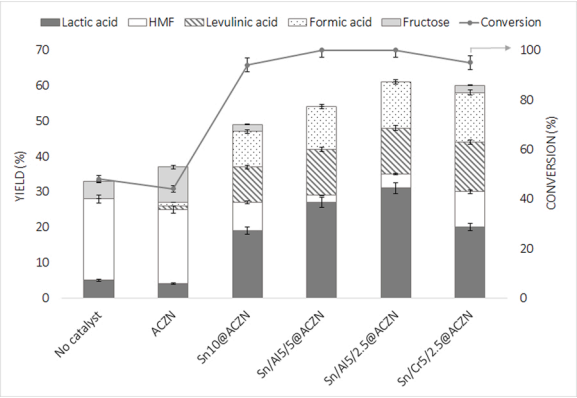

Fig. 3. Glucose conversion and product yields with AC_{ZN} catalysts after 120 min at 180 °C, 30 bar, and 500 rpm, using 0.1 g of catalyst and 0.1 g of glucose in 20 mL of H_2O (Z = chemical act., N = HNO_3 treat).

sample.

After two hours, without a catalyst in the reaction system, the conversion of glucose was 48 %, and HMF was the main synthesis product with a yield of 23 % with a minor lactic acid yield of 5%. When AC_{ZN} was added in the reaction, a slightly higher fructose yield was noticed; however, the lactic acid and HMF yield was about the same as that without the catalyst. With the addition of 10 wt.% of tin to the support (corresponding to 0.084 mmol of Sn in 0.1 g of catalyst), the conversion was almost complete (94 %) and the formation of lactic acid increased to 19 % with $Sn_{10}@AC_{ZN}$. Results indicated that the presence of SnO_2 in the support promotes the conversion of glucose and the formation of lactic acid instead of HMF. With the addition of aluminum at 5 wt.% with 5 wt. % of tin (0.042 mmol of Sn and 0.19 mmol of Al), the lactic acid yield increased to 27 %, and complete conversion of glucose was achieved with the $Sn/Al_{5/5}@AC_{ZN}$ catalyst. However, when the aluminum/tin ratio was changed to 5/2.5 wt.% (0.042 mmol of Sn and 0.093 mmol of Al), the highest lactic acid yield (31 %) was reached with the $Sn/Al_{5/2.5}@AC_{ZN}$ catalyst. The trend indicated that the addition of a small amount of Al improved the formation of lactic acid, while the higher loading did not improve it further. Deng et al. noticed that for homogeneous catalysts, selectivity for lactic acid was highest when the molar ratio of Sn/(Sn + Al) was 0.5, and it decreased for lower or higher ratios [16]. In our studies, we see a similar trend, with lactic acid yield decreasing in the order $Sn/Al_{5/2.5}@AC_{ZN}$ > $Sn/Al_{5/5}@AC_{ZN}$ > $Sn_{10}@AC_{ZN}$, where the Sn/(Sn + Al) molar ratio was 0.30, 0.19, and 1.00, respectively. Lewis acids, such as tin, are found to catalyze the isomerization of glucose into fructose, as well as the retro-aldol reaction of hexoses into trioses [10,26] (see Scheme 1). Other research groups have studied glucose conversion with supported $Sn10/\gamma\text{-}Al_2O_3$ catalysts that yielded 20 % lactic acid and 25 % HMF [26]. Holm et al. tested Sn-zeolites and obtained a lactic acid yield of 26 % in a water solution [10]. Aluminum oxide was also used as a solid Lewis acid catalyst for converting trioses, with a lactic acid yield of 28 % [27]. Rasrendra et al. found that the aluminum and chromium metal salts were the most active catalysts converting trioses such as dihydroxyacetone and glyceraldehyde to lactic acid in water [19]. Takagaki et al. found that a chromium oxide catalyst could easily transform pyruvaldehyde to lactic acid, with a yield of 46 % [22]. Xia et al. found that the Cr/(Cr:Sn) molar ratio of 0.5 on a Cr-Sn-Beta zeolite gave the highest yield of lactic acid in the conversion of glucose [58]. However, in this study, the addition of chromium oxide with tin oxide to the $Sn/Cr_{5/2.5}@AC_{ZN}$ catalyst (0.042 mmol of Sn and 0.044 mmol of Cr, at a molar ratio of 0.5), did not improve the production of lactic acid, as compared to the Sn/Al catalyst. Instead, the addition of chromium oxide seemed to direct the reaction towards the production of HMF and levulinic acid, in contrast to the Sn/Al catalyst.

To conclude, the highest yield of lactic acid produced was with the combination of Sn with Al, at a ratio of 5:2.5 (Sn/Al wt.%) on AC_{ZN}. This combination was selected for use in the following examinations for conversion of glucose to lactic acid.

3.2.3. *Effect of the catalyst support*

The effect of the catalyst support on the conversion of glucose to lactic acid was studied at 180 °C, 30 bar, 500 rpm using 0.100 g of the catalyst (0.042 mmol of Sn and 0.093 mmol of Al) and 0.100 g of the glucose in 20 ml of H_2O. The activated carbon supports AC_S, AC_{SN}, AC_Z, and AC_{ZN} were tested as reference samples (treated in an N_2-atmosphere at 350 °C for 3 h similar to the catalysts). The supports were impregnated with the Sn/Al catalyst at a ratio of 5/2.5 wt.%. AC_Z was used as a support only after treating it with nitric acid, since it contained 5 wt.% zinc (see Table S2). The results of the conversion and main product yields are presented in Fig. 4. Other byproduct yields were not quantified.

After two hours, the conversion of glucose in the batch system for AC_{SN} and AC_{ZN} reached about the same conversion rate as that without the catalyst (Fig. 3), and no notable differences in the yield of lactic acid were observed. With AC_S, a higher conversion rate was noticed, but the lactic acid yield was about the same as before. Furthermore, slightly higher fructose and HMF yields were noticed with an increasing order of $AC_S < AC_{SN} < AC_{ZN}$, which was in the same order as the increase in total acidity of the ACs (see Table 2). This could be due to the Brønsted acids (acidic groups) on the ACs, which can catalyze fructose to HMF and its derivatives [59]. In contrast, AC_Z yielded 27 % lactic acid and a 97 % conversion rate, and the HMF yield shifted to levulinic acid. It was found that ZnO in the support (see ICP-OES, XRD, and XPS results) can act as a catalyst and convert glucose to lactic acid [15,34]. However, AC_Z was not used as a support for Sn/Al without treating it first with nitric acid to remove residual ZnO as it already contained the active metal oxide.

With the addition of Sn and Al oxides to the AC_S support, the $Sn/Al_{5/2.5}@AC_S$ catalyst provided glucose conversion of 98 % and a lactic acid yield of 24 %. With the acid-treated Sn/Al-catalysts, the glucose conversion rate reached 100 % and the highest lactic acid yields of 31 % and 34 % were reached with the $Sn/Al_{5/2.5}@AC_{ZN}$ and $Sn/Al_{5/2.5}@AC_{SN}$ catalysts, respectively. Also, there was a shift from HMF to levulinic acid as the main byproduct. Results indicated that nitric acid treatment of the catalyst support had an impact on the conversion of glucose to lactic acid, seen in comparison to the untreated catalyst support ($Sn/Al_{5/2.5}@AC_S$). Further analysis of the reaction mixture was performed with GC—MS. GCM—S chromatograms and MS spectra (Fig. S8 and S9, Supplementary material) revealed that lactic acid was the main product with all catalysts. Also, other monocarboxylic acids such as formic acid and acetic acid were identified from the product mixture. With more acidic catalysts ($Sn/Al_{5/2.5}@AC_{SN}$ and $Sn/Al_{5/2.5}@AC_{ZN}$) byproducts formed besides the HMF and levulinic acid were other furfural

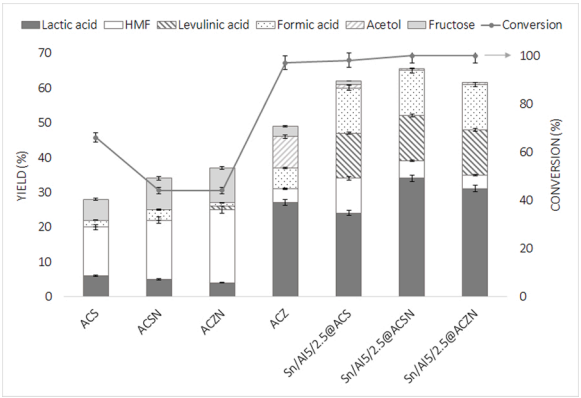

Fig. 4. Glucose conversion and product yields with AC and Sn/Al catalysts after 120 min at 180 °C, 30 bar, and 500 rpm using 0.1 g of catalyst and 0.1 g of glucose in 20 mL of H_2O (Z = chemical act., S = steam act., N = HNO_3 treat).

derivatives such as 5-methyl furfural and 2,5-furandicarboxaldehyde and amount of byproducts varied during the reaction time (Fig. S10, Supplementary material). Compounds such as dihydroxyacetone, glyceraldehyde were also identified from the product mixture indicating that reaction towards lactic acid was going through the formation of dihydroxyacetone as intermediate (Fig. S10). The main byproduct with AC_Z catalyst was identified as acetol (hydroxyacetone) (Fig. S8). It has been found that acetol and lactic acid are formed competitively from the same intermediate, i.e. pyruvaldehyde, via hydrogenation on metal surfaces [60–62]. Without the presence of external hydrogen in the reaction system, the hydrogenation can occur via transfer hydrogenation by hydrogen donor such as formic acid for example [63]. With AC_Z, the acetol production was prominent compared to more acidic Sn/Al catalysts, which on the other hand, directed the reaction towards HMF and its derivative's production. Other byproducts formed such gaseous products or humines in the reaction mixture were not analyzed. It has been claimed that Lewis acid sites on heterogeneous catalysts are crucial for lactic acid production, while the Brønsted acid sites play no role at all [64]. Rasrendra et al. found that Brønsted acids, namely H^+ ions, had a positive effect on the conversion of dihydroxyacetone to pyruvaldehyde while Lewis acid sites played a key role with conversion of trioses to lactic acid [65]. Clippel et al. studied dihydroxyacetone conversion to lactic acid and it's esters with bifunctional carbon-silica catalysts and demonstrated that the presence of weak Brønsted acid sites originating from oxygen-containing functional groups in the carbon part were crucial in accelerating the dehydration reaction [66]. This indicated that acidic sites on the carbon surface could participate on the conversion of dihydroxyacetone to pyruvaldehyde and further to higher yields of lactic acid, explaining why more acidic $Sn/Al_{5/2.5}@AC_{SN}$ was performing better than less acidic $Sn/Al_{5/2.5}@AC_S$ (see chapter 3.1.1). Furthermore, when comparing $Sn/Al_{5/2.5}@AC_{SN}$ and $Sn/Al_{5/2.5}@AC_{ZN}$, the higher acidic group concentration on AC_{ZN} compared to AC_{SN} did not seem to have notable effect on the conversion rate or the lactic acid yield or on changes in the byproduct yields after addition of Sn/Al. The higher SA of the $Sn/Al_{5/2.5}@AC_{ZN}$ catalyst also did not seem to contribute to the higher activity or lactic acid yield for the catalyst, as compared to the steam-activated $Sn/Al_{5/2.5}@AC_{SN}$ with a lower SA. Both catalysts had almost similar mesoporous structures, indicating that having a more microporous structure is not beneficial for lactic acid production. It is possible that the molecules are too big to fit in the smallest micropores, or that the desorption of the products is difficult. This could be also the reason why higher acidic group concentration on the $Sn/Al_{5/2.5}@AC_{ZN}$ did not have an effect on the conversion rate or the lactic acid yield if the active acidic sites in the smallest micropores were not accessible for the reactants or were blocked. It has been shown that oxidized carbon catalysts, specially carboxylic groups on carbon, take place in dehydration reactions, however, not only the number of the acidic groups but also their location and accessibility are relevant for the reaction [67–69]. Results indicated that the environmentally hazardous $ZnCl_2$ treatment step could be removed from the pretreatment process of the AC support, since the more microporous surface has no beneficial role to play in the conversion process or in the yield of lactic acid after the addition of Sn/Al to the support. Even though, it was noted that presence of ZnO and a lower amount of acidic groups in the catalyst seemed to produce lactic acid and inhibit the formation of HMF and its derivatives, the addition of Sn/Al oxides on acidified catalyst support resulted in the best lactic acid production levels. Moreover, the addition of zinc on the support cannot be controlled since it is left over from the activation process. Detailed studies regarding the preparation of carbon-supported zinc oxide catalysts and their utilization in lactic acid production are ongoing and will be reported at a later date.

Based on the discussion above, we propose a reaction route presented in Scheme 2. as the reaction pathway for production of lactic acid and main byproducts with the AC based catalyst. The detailed reaction mechanism remains in question at the moment.

3.2.4. *Catalyst optimization studies*

Based on studies of the effect of metal and support interactions on glucose conversion to lactic acid, the $Sn/Al_{5/2.5}@AC_{SN}$ catalyst was selected for optimization studies in the aqueous phase. The effects of catalyst loading, time, temperature, and pressure on the conversion of glucose to lactic acid were studied. Glucose at a concentration of 0.100 g was used and mixed at 500 rpm in 20 ml of H_2O in all the experiments. The effect of catalyst loading at a temperature of 180 °C, with increasing catalyst amounts (0.050, 0.100, 0.150, and 0.200 g) was studied (Fig. 5). A catalyst load of 0.050 g was too low, as 100 % conversion of glucose was not achieved even after 3 h. With higher catalyst loading ($\geq$ 0.100 g), the glucose conversion rate reached 100 % within 60 min, and a catalyst concentration of 0.100 g yielded 34 % of lactic acid. Using 0.150 g of the $Sn/Al_{5/2.5}@AC_{SN}$ catalyst, a yield of 37 % was achieved after 30 min. The highest yield of lactic acid (42 %) was achieved in 30 min using 0.200 g of the catalyst, and the yield was constant even at a reaction time of 180 min. An overview of some of the used heterogeneous catalysts in the conversion of biomass to lactic acid is presented in Table 3. Comparing our results to those, our catalyst provided reasonable yields of lactic acid in glucose conversion.

The effect of the reaction temperature on the conversion of glucose to lactic acid was studied at 160, 180 and 200 °C using 0.200 g of the $Sn/Al_{5/2.5}@AC_{SN}$ catalyst and 30 bar reaction pressure (Fig. 6). The complete conversion of glucose at 160 °C took 120 min to achieve and was slower than at higher temperatures (180 and 200 °C) where the reaction rate increased and conversion was almost complete ($\geq$ 98 %) at 20 min. Besides, the increase in the lactic acid yield from 35 % to 42 % was detected when the temperature was increased from 160 °C to 180 °C, but a further increase in the temperature did not increase the lactic acid yield. During the reaction temperature increase, byproducts (HMF and

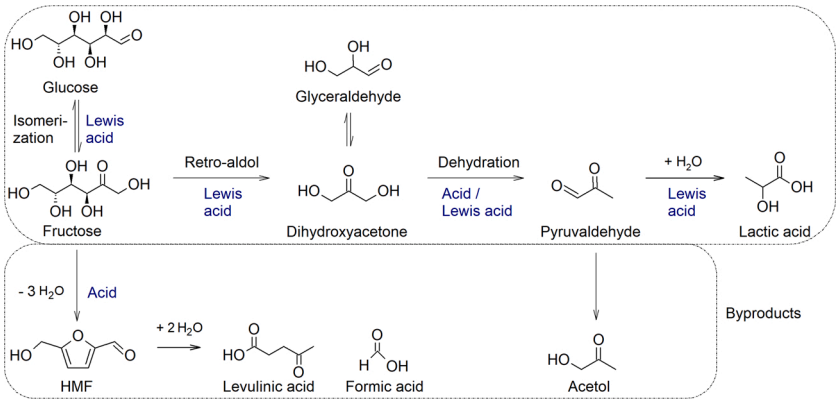

Scheme 2. Proposed reaction pathway for the production of lactic acid and main byproducts formed with AC based catalysts [15,66].

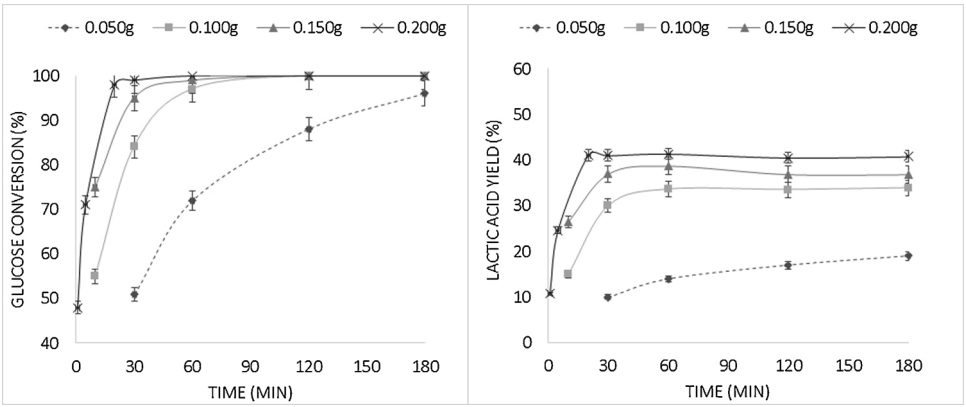

Fig. 5. Effect of catalyst load on the conversion of glucose to lactic acid after 180 min at 180 °C and 30 bar, using 0.050 g, 0.100 g, 0.150 g, and 0.200 g of the Sn/$Al_{5/2.5}$@AC_{SN} catalyst (0.1 g glucose in 20 mL H_2O).

Table 3
Overview of the heterogeneous catalysts used in the conversion of biomass to lactic acid.

Catalyst	Substrate	Conditions in conversion	Yield of lactic acid	Ref.
γ-AlO(OH)	Glucose (0.28 mmol)	H_2O (3 mL); 170 °C; 24 h; cat. 50 mg	~30 %	[27]
SnO_2 Sn20/ γ-Al2O_3	Glucose (4% wt.)	H_2O; 150 °C; 1 h; N_2; cat: subs 1:1 w/w	<20 %	[26]
SnO_2	Glucose (1.25 mmol)	H_2O (10 mL); 190 °C; 2 h; cat. 160 mg	6%	[15]
ZnO			12 %	
Sn-Beta			23 %	
Zn-Sn-Beta			48 %	
Pb-Sn-Beta	Glucose (1.25 mmol)	H_2O (10 mL); 190 °C; 2 h; air; cat. 200 mg.	52 %	[25]
Sn-Beta	Sucrose (1.25 mmol)	H_2O (8.0 g); 160 °C; 20 h; cat. 160 mg	<30 %	[10]
Pt/C	Glucose (0.25 mmol)	H_2O (5 mL); 80 °C; 2 h; NaOH (1 mol L^{-1}); cat. 50 mg	43 %	[30]
Sn/$Al_{5/2.5}$@AC_{SN}	Glucose (0.55 mmol)	H_2O (20 mL); 180 °C; N_2; 20 min; cat. 200 mg	42 %	This study

levulinic acid) were formed faster (Fig. S11, Supplementary material). At 200 °C, the color of the reaction solution was much darker (Fig. S12, Supplementary material), even though the lactic acid yield was not higher, indicating that other, unwanted soluble byproducts (including polymeric materials, such as humines) could have formed from the decomposition of reaction products at higher temperatures [22]. This suggested that a temperature of 180 °C was optimum for the reaction and a further increase in temperature was unfavorable for the selectivity of the reaction.

Different types of atmospheres notably influence the yields of lactic acid, and an atmosphere of pure nitrogen was found to yield the highest amount of lactic acid compared to oxygen and air [70,71]. Sun et al. found that an increase in pressure gave higher lactic acid yields up to 40 bar (He), after which the yield started to decrease [72]. An atmosphere of nitrogen was used in our catalytic studies. The effect of increasing pressure on the conversion rate and the yield of lactic acid was tested at ~5, 20, 30, and 40 bar. The pressure increase was carried out by the addition of inert gas (N_2) into the system. The pressure of the reaction itself was about five bar, when no excess pressure was added. As seen in Fig. 7, the pressure increase from 5 to 40 bar did not seem to have a major effect on either the conversion rate or the yield of lactic acid. A slightly lower conversion rate was noted after 20 min when no pressure was added, but the difference was only 4%, and after 60 min, the conversion rate was 100 % for all pressures. The lactic acid yield was about the same at every tested pressure. This was noted as a positive result since excess pressure does not need to be added to the system.

3.2.5. *Reusability tests*

Reusability tests of the Sn/$Al_{5/2.5}$@AC_{SN} catalyst were performed to obtain information about the stability of the catalyst. Tests were performed at 180 °C, at 5 bar (pressure of the reaction itself) and 30 bar with 0.2 g of the catalyst and 0.1 g of glucose in 20 ml of H_2O. The catalyst was filtered after 120 min, washed with ethanol, dried in the oven at 105 °C, and tested in the same conditions as in the first run at four cycles. Ethanol wash was selected instead of water after reuse, as the lower-polarity solvent could access the catalyst pores easier. As a result of the reuse (Fig. 8), glucose conversion decreased from 100 % to

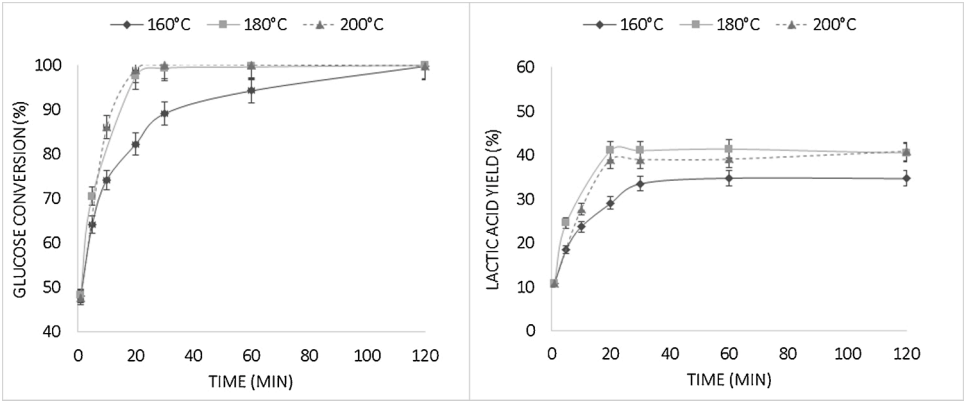

Fig. 6. Effect of temperature on the conversion glucose to lactic acid after 120 min at 160 °C, 180 °C, and 200 °C, using 0.2 g of the Sn/$Al_{5/2.5}$@AC_{SN} catalyst at 30 bar (0.1 glucose in 20 mL H_2O).

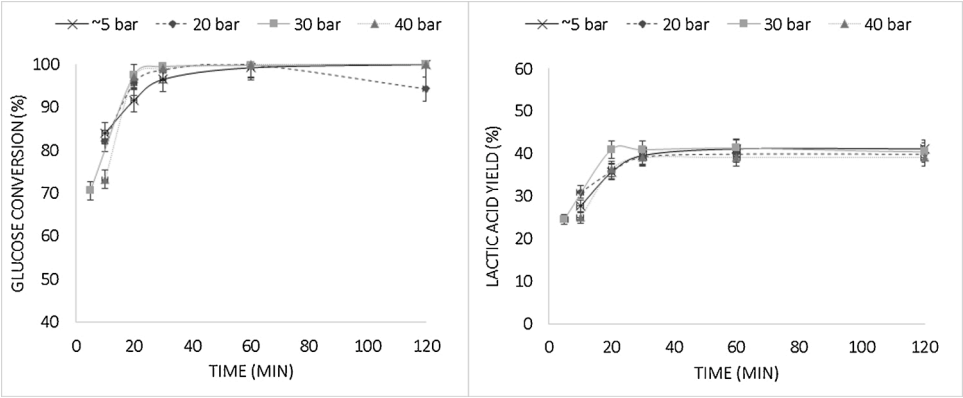

Fig. 7. The effect of pressure on the conversion of glucose to lactic acid after 120 min at ~5, 20, 30, and 40 bar, using 0.2 g of the $Sn/Al_{5/2.5}@AC_{SN}$ catalyst at 180 °C (0.1 g glucose in 20 mL H_2O).

86 % after the first cycle, and finally to 80 % after four cycles. Yield of lactic acid decreased from about 40 % after the first cycle to 15 % after four cycles. More fructose was detected in the reaction solution, indicating the reaction was not completed, and yield of HMF increased from 5% to 15 %. No differences were detected in the conversion rates and yields at the different reaction pressures used (~5 to 30 bar).

After catalyst reuse, the reaction liquid was analyzed using the ICP-OES method, and the metal content was determined after each recycle of the catalyst. The hot, acidic medium can promote the solubility of some metal oxides and cause deactivation of the heterogeneous catalysts by leaching the metal or metal oxides [73]. In these experiments, the pH of the final product solution was about 2. After the first run, 0.2 % of tin was leached from the initial amount of Sn added to the catalyst; 15 % of aluminum was leached from the initial metal content added to the catalyst. After the second run, leaching was 0% for Sn and 1.0 % for aluminum. This indicated that some of the Al was leaching; however, it was relatively minor, and Sn was quite stable on the catalyst. The SA and the pore volumes of the catalyst were also determined after four recycles. The BET SA of the catalyst was 97 $m^2\ g^{-1}$, with a pore volume of 0.06 $cm^3\ g^{-1}$, resulting in an 82 % decrease of the BET SA and a 75 % decrease of the pore volume, leading to the conclusion that most of the SA and porosity was lost during the use of the catalyst. Blocking of the catalytic sites on the porous structure of catalyst by adsorbed reaction products or carbon deposits seems to be the cause of the catalyst deactivation. Moreover, the product distribution after fourth reuse seems to be similar as with the plain AC support, indicating blocking of the active metal sites on catalyst support. In the aqueous solution, carbonaceous byproducts, such as humines, can be formed during the reaction, which can block the pores, deposit on the active sites, and finally deactivate the catalyst [66,74,75]. In other research, calcination at mild conditions was used successfully to reactivate the catalyst after residue deposition [76]. After fourth reuse, the catalyst was calcined in air at 300 °C for two hours to remove the deposits on the catalyst surface. After calcination, The BET SA of the catalyst was 640 $m^2\ g^{-1}$, indicating that the pore structure was opened. However, lactic acid yield was the same as after second reuse (Fig. 8), suggesting that leaching of aluminum was also the reason for decrease in lactic acid yield after reuse. This verified the fact that co-operation of the two metals; tin and aluminum was important for the catalyst selectivity to lactic acid.

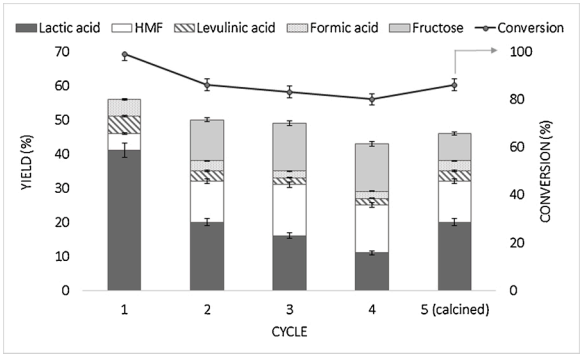

Fig. 8. Reusability of the $Sn/Al_{5/2.5}@AC_{SN}$ catalyst five times during the conversion of glucose to lactic acid, after 120 min at ~5 bar, using 0.2 g of the catalyst at 180 °C (0.1 g glucose in 20 mL H_2O). After fourth cycle, the catalyst was calcined in air at 300 °C for 2h.

4. Conclusions

The aim of this work was to illustrate the possibility to utilize lignocellulosic side stream, hydrolysis lignin as a raw material for activated carbon, which in turn could be used as catalyst support for metal oxide catalysts. The modification of the AC support by chemical treatments with $ZnCl_2$ and HNO_3 was also studied. The prepared lignin-based activated carbon-supported tin-, aluminum- or chromium-containing catalysts were studied in the conversion reaction of glucose to lactic acid. All of the tested carbon-supported metal oxide catalysts showed a high rate of glucose conversion (> 94 %) and were able to convert glucose to lactic acid in 20–120 min, depending on the reaction conditions. The addition of tin oxide along with aluminum oxide resulted in higher lactic acid production yields, in contrast to chromium oxide, which directed the reaction towards byproduct formation. It was noted that activated carbon support prepared by chemical activation with zinc chloride caused the deposition of zinc oxides on the support; this by itself was able to convert glucose to lactic acid and should be studied more in the future. Moreover, treatment of the AC surface with nitric acid had a positive effect on the lactic acid yield when tin and aluminum oxides were added on to the support, and was related to the higher acidity of the catalyst. The highest yield of lactic acid was produced with steam-activated and nitric acid-treated carbon support containing Sn/Al oxides at 5/2.5 wt.% ($Sn/Al_{5/2.5}@AC_{SN}$)—within 20 min, the catalyst $Sn/Al_{5/2.5}@AC_{SN}$ yielded 42 % lactic acid at 180 °C without addition of excess pressure. However, the reusability experiments indicated that the catalyst was not stable in an aqueous solution, resulting in a decrease in lactic acid yield within four cycles. This was probably caused by the deposition of carbonaceous byproducts, such as humines, on the catalyst active sites and leaching of aluminum oxides as active metal. In conclusion, lignin-based activated carbon supports provided interesting results and opened a window for later studies with lactic acid production. Furthermore, improved catalyst and reaction condition design is needed for better selectivity and to obtain the recyclable catalyst without deactivation.

CRediT authorship contribution statement

Riikka Kupila: Conceptualization, Investigation, Formal analysis, Writing - original draft. **Katja Lappalainen:** Conceptualization, Supervision, Writing - review & editing. **Tao Hu:** Formal analysis, Writing - review & editing. **Henrik Romar:** Writing - review & editing. **Ulla Lassi:** Supervision, Writing - review & editing.

Declaration of Competing Interest

The authors declare no conflict of interest.

Acknowledgements

Authors R.K. and K.L. would like to thank the Green Bioraff Solutions Project (EU/Interreg/Botnia-Atlantica, 20201508) for funding this research. Hanna Prokkola is thanked for performing the elemental analysis. Mia Pirttimaa and Sari Tuikkanen are thanked for methods developed with HPLC analytics.

Appendix A. Supplementary data

Supplementary material related to this article can be found, in the online version, at doi:https://doi.org/10.1016/j.apcata.2021.118011.

References

[1] M. Dusselier, P. Van Wouwe, A. Dewaele, E. Makshina, B.F. Sels, Energy Environ. Sci. 6 (2013) 1415–1442, https://doi.org/10.1039/C3EE00069A.
[2] F.A. Castillo Martinez, E.M. Balciunas, J.M. Salgado, J.M. Domínguez González, A. Converti, R.P. de S. Oliveira, Trends Food Sci. Technol. 30 (2013) 70–83, https://doi.org/10.1016/J.TIFS.2012.11.007.
[3] Y. Fan, C. Zhou, X. Zhu, Catal. Rev. 51 (2009) 293–324, https://doi.org/10.1080/01614940903048513.
[4] R. Datta, M. Henry, J. Chem. Technol. Biotechnol. 81 (2006) 1119–1129, https://doi.org/10.1002/jctb.1486.
[5] S. Li, W. Deng, Y. Li, Q. Zhang, Y. Wang, J. Energy Chem. 32 (2019) 138–151, https://doi.org/10.1016/J.JECHEM.2018.07.012.
[6] C. Gao, C. Ma, P. Xu, Biotechnol. Adv. 29 (2011) 930–939, https://doi.org/10.1016/J.BIOTECHADV.2011.07.022.
[7] A. Djukić-Vuković, D. Mladenović, J. Ivanović, J. Pejin, L. Mojović, Renew. Sustain. Energy Rev. 108 (2019) 238–252, https://doi.org/10.1016/J.RSER.2019.03.050.
[8] R.P. John, K.M. Nampoothiri, A. Pandey, Appl. Microbiol. Biotechnol. 74 (2007) 524–534, https://doi.org/10.1007/s00253-006-0779-6.
[9] E. Cubas-Cano, C. González-Fernández, M. Ballesteros, E. Tomás-Pejó, Biofuels, Bioprod. Biorefining. 12 (2018) 290–303, https://doi.org/10.1002/bbb.1852.
[10] M.S. Holm, S. Saravanamurugan, E. Taarning, Science (80-.) 328 (2010) 602–605, https://doi.org/10.1126/science.1183990.
[11] A. Corma, S. Iborra, A. Velty, Chem. Rev. 107 (2007) 2411–2502, https://doi.org/10.1021/cr050989d.
[12] R. Sindhu, A. Pandey, Bioresour. Technol. 199 (2016) 76–82, https://doi.org/10.1016/J.BIORTECH.2015.08.030.
[13] P. Mäki-Arvela, I.L. Simakova, T. Salmi, D.Y. Murzin, Chem. Rev. 114 (2014) 1909–1971, https://doi.org/10.1021/cr400203v.
[14] P. Wattanapaphawong, P. Reubroycharoen, A. Yamaguchi, RSC Adv. 7 (2017) 18561–18568, https://doi.org/10.1039/C6RA28568F.
[15] W. Dong, Z. Shen, B. Peng, M. Gu, X. Zhou, B. Xiang, Y. Zhang, Sci. Rep. 6 (2016), 26713, https://doi.org/10.1038/srep26713.
[16] W. Deng, P. Wang, B. Wang, Y. Wang, L. Yan, Y. Li, Q. Zhang, Z. Cao, Y. Wang, Green Chem. 20 (2018) 735–744, https://doi.org/10.1039/c7gc02975f.
[17] Z. Huo, Y. Fang, D. Ren, S. Zhang, G. Yao, X. Zeng, F. Jin, ACS Sustain. Chem. Eng. 2 (2014) 2765–2771, https://doi.org/10.1021/sc500507b.
[18] Y. Wang, W. Deng, B. Wang, Q. Zhang, X. Wan, Z. Tang, Y. Wang, C. Zhu, Z. Cao, G. Wang, H. Wan, Nat. Commun. 4 (2013) 2141, https://doi.org/10.1038/ncomms3141.
[19] C.B. Rasrendra, I.G.B.N. Makertihartha, S. Adisasmito, H.J. Heeres, Top. Catal. 53 (2010) 1241–1247, https://doi.org/10.1007/s11244-010-9570-0.
[20] S. Zhang, F. Jin, J. Hu, W. Zhang, J. Chem. Technol. Biotechnol. 92 (2017) 1046–1052, https://doi.org/10.1002/jctb.5080.
[21] P. Sudarsanam, R. Zhong, S. den Bosch, S.M. Coman, V.I. Parvulescu, B.F. Sels, Chem. Soc. Rev. 47 (2018) 8349–8402, https://doi.org/10.1039/C8CS00410B.
[22] A. Takagaki, H. Goto, R. Kikuchi, S.T. Oyama, Appl. Catal. A Gen. 570 (2019) 200–208, https://doi.org/10.1016/J.APCATA.2018.11.018.
[23] T.V. dos Santos, D.O. da Silva Avelino, M.R. Meneghetti, S.M.P. Meneghetti, Catal. Commun. 114 (2018) 120–123, https://doi.org/10.1016/J.CATCOM.2018.06.019.
[24] N. Shi, Q. Liu, X. He, H. Cen, R. Ju, Y. Zhang, L. Ma, Bioresour. Technol. Reports. 5 (2019) 66–73, https://doi.org/10.1016/J.BITEB.2018.12.005.
[25] M. Xia, W. Dong, M. Gu, C. Chang, Z. Shen, Y. Zhang, RSC Adv. 8 (2018) 8965–8975, https://doi.org/10.1039/C7RA12533J.
[26] A.A. Marianou, C.M. Michailof, A. Pineda, E.F. Iliopoulou, K.S. Triantafyllidis, A. A. Lappas, Appl. Catal. A Gen. 555 (2018) 75–87, https://doi.org/10.1016/J.APCATA.2018.01.029.
[27] A. Takagaki, J.C. Jung, S. Hayashi, RSC Adv. 4 (2014) 43785–43791, https://doi.org/10.1039/C4RA08061K.
[28] C. Zhang, T. Wang, X. Liu, Y. Ding, Chin. J. Catal. 37 (2016) 502–509, https://doi.org/10.1016/S1872-2067(15)61055-5.
[29] F.L. Marques, A.C. Oliveira, J. Mendes Filho, E. Rodríguez-Castellón, C. L. Cavalcante, R.S. Vieira, Fuel Process. Technol. 138 (2015) 228–235, https://doi.org/10.1016/J.FUPROC.2015.05.032.
[30] A. Onda, T. Ochi, K. Kajiyoshi, K. Yanagisawa, Appl. Catal. A Gen. (2008), https://doi.org/10.1016/j.apcata.2008.03.017.
[31] E. Pérez-Mayoral, V. Calvino-Casilda, E. Soriano, Catal. Sci. Technol. 6 (2016) 1265–1291, https://doi.org/10.1039/C5CY01437A.
[32] K. Pirkanniemi, M. Sillanpää, Chemosphere. 48 (2002) 1047–1060, https://doi.org/10.1016/S0045-6535(02)00168-6.
[33] J. Schönherr, J.R. Buchheim, P. Scholz, P. Adelhelm, C–J. Carbon Res. 4 (2018), https://doi.org/10.3390/c4020021.
[34] H.P. Boehm, J. Adv. Catal. Sci. Technol. 16 (1966) 179–274, https://doi.org/10.1016/S0360-0564(08)60354-5.
[35] A.M. Oickle, S.L. Goertzen, K.R. Hopper, Y.O. Abdalla, H.A. Andreas, Carbon 48 (2010) 3313–3322, https://doi.org/10.1016/j.carbon.2010.05.004.
[36] C. Moreno-Castilla, M.A. Ferro-Garcia, J.P. Joly, I. Bautista-Toledo, F. Carrasco-Marin, J. Rivera-Utrilla, Langmuir 11 (1995) 4386–4392, https://doi.org/10.1021/la00011a035.
[37] C. Moreno-castilla, F. Carrasco-marín, F.J. Maldonado-hódar, J. Rivera-utrilla, Carbon 36 (1998) 145–151, https://doi.org/10.1016/S0008-6223(97)00171-1.
[38] X. Song, H. Liu, L. Cheng, Y. Qu, Desalination 255 (2010) 78–83, https://doi.org/10.1016/J.DESAL.2010.01.011.
[39] P. Munnik, P.E. de Jongh, K.P. de Jong, Chem. Rev. 115 (2015) 6687–6718, https://doi.org/10.1021/cr500486u.
[40] J.L. Figueiredo, M.F.R. Pereira, Catal. Today 150 (2010) 2–7, https://doi.org/10.1016/j.cattod.2009.04.010.
[41] N. Chubar, V. Gerda, M. Micusik, M. Omastová, K. Heister, P. Man, G. Yablokova, D. Banerjee, J. Fraissard, Acta Phys. Pol. A. 133 (2018) 1091–1096, https://doi.org/10.12693/APhysPolA.133.1091.
[42] Z. Cao, C. Zuo, RSC Adv. 7 (2017) 40243–40248, https://doi.org/10.1039/C7RA06188A.
[43] Y.-C. Liang, C.-C. Wang, RSC Adv. 8 (2018) 5063–5070, https://doi.org/10.1039/C7RA13061A.
[44] J. Schönherr, J. Buchheim, P. Scholz, P. Adelhelm, J. Carbon Res. 4 (2018) 22, https://doi.org/10.3390/c4020022.
[45] U. Zielke, K.J. Hüttinger, W.P. Hoffman, Carbon 34 (1996) 983–998, https://doi.org/10.1016/0008-6223(96)00032-2.
[46] S. Biniak, G. Szymański, J. Siedlewski, A. Świątkowski, Carbon 35 (1997) 1799–1810, https://doi.org/10.1016/S0008-6223(97)00096-1.
[47] P. Burg, P. Fydrych, D. Cagniant, G. Nanse, J. Bimer, A. Jankowska, Carbon 40 (2002) 1521–1531, https://doi.org/10.1016/S0008-6223(02)00004-0.
[48] J. Liqiang, W. Dejun, W. Baiqi, L. Shudan, X. Baifu, F. Honggang, S. Jiazhong, J. Mol. Catal. A Chem. 244 (2006) 193–200, https://doi.org/10.1016/j.molcata.2005.09.020.
[49] W. Qi, W. Liu, B. Zhang, X. Gu, X. Guo, D. Su, Angew. Chemie Int. Ed. 52 (2013) 14224–14228, https://doi.org/10.1002/anie.201306825.
[50] S. Wu, G. Wen, R. Schlögl, D. Su, Phys. Chem. Chem. Phys. 17 (2014), https://doi.org/10.1039/c4cp04658g.
[51] J.L. Figueiredo, M.F.R. Pereira, M.M.A. Freitas, J.J.M. Órfão, Carbon 37 (1999) 1379–1389, https://doi.org/10.1016/S0008-6223(98)00333-9.
[52] Y.F. Jia, K.M. Thomas, Langmuir 16 (2000) 1114–1122, https://doi.org/10.1021/la990436w.
[53] I.I. Salame, T.J. Bandosz, J. Colloid Interface Sci. 240 (2001) 252–258, https://doi.org/10.1006/jcis.2001.7596.
[54] R. Tian, Y. Zhang, Z. Chen, H. Duan, B. Xu, Y. Guo, H. Kang, H. Li, H. Liu, Sci. Rep. 6 (2016), 19195, https://doi.org/10.1038/srep19195.
[55] M. Kwoka, B. Lyson-Sypien, A. Kulis, D. Zappa, E. Comini, Nanomaterials 8 (2018) 738, https://doi.org/10.3390/nano8090738.
[56] L. Nie, A. Meng, J. Yu, M. Jaroniec, Sci. Rep. 3 (2013) 3215, https://doi.org/10.1038/srep03215.
[57] B. Singh, M. Camps-Arbestain, J. Lehmann, CSIRO (Australia), Biochar: A Guide to Analytical Methods, 2017. https://books.google.co.uk/books?hl=en&lr=&id=ieRrDgAAQBAJ&oi=fnd&pg=PP1&dq=biochar:+a+guide+to+analytical+methods&ots=zBBO1rVDD7&sig=ysnb7inmaSDYu1EHCJSbOkejehg&redir_esc=y#v=onepage&q&f=false.
[58] M. Xia, Z. Shen, S. Xiao, B. Peng, M. Gu, W. Dong, Y. Zhang, Appl. Catal. A Gen. 583 (2019), 117126, https://doi.org/10.1016/j.apcata.2019.117126.
[59] G. Yang, E.A. Pidko, E.J.M. Hensen, J. Catal. 295 (2012) 122–132, https://doi.org/10.1016/j.jcat.2012.08.002.
[60] Y. Hirano, K. Sagata, Y. Kita, Appl. Catal. A Gen. 502 (2015) 1–7, https://doi.org/10.1016/j.apcata.2015.05.008.
[61] T. Deng, H. Liu, J. Mol. Catal. A Chem. 388–389 (2014) 66–73, https://doi.org/10.1016/j.molcata.2013.11.016.
[62] T. Deng, H. Liu, Green Chem. 15 (2013) 116–124, https://doi.org/10.1039/C2GC36088H.
[63] S.H. Hakim, B.H. Shanks, J.A. Dumesic, Appl. Catal. B Environ. 142–143 (2013) 368–376, https://doi.org/10.1016/j.apcatb.2013.05.021.

[64] K.M.A. Santos, E.M. Albuquerque, L.E.P. Borges, M.A. Fraga, Mol. Catal. (2018), https://doi.org/10.1016/j.mcat.2017.12.010.
[65] C.B. Rasrendra, B.A. Fachri, I.G.B.N. Makertihartha, S. Adisasmito, H.J. Heeres, ChemSusChem. 4 (2011) 768–777, https://doi.org/10.1002/cssc.201000457.
[66] F. de Clippel, M. Dusselier, R. Van Rompaey, P. Vanelderen, J. Dijkmans, E. Makshina, L. Giebeler, S. Oswald, G.V. Baron, J.F.M. Denayer, P.P. Pescarmona, P.A. Jacobs, B.F. Sels, J. Am. Chem. Soc. 134 (2012) 10089–10101, https://doi.org/10.1021/ja301678w.
[67] G.S. Szymański, Z. Karpiński, S. Biniak, A. Świątkowski, Carbon 40 (2002) 2627–2639, https://doi.org/10.1016/S0008-6223(02)00188-4.
[68] F. Carrasco-Marín, A. Mueden, C. Moreno-Castilla, J. Phys. Chem. B 102 (1998) 9239–9244, https://doi.org/10.1021/jp9818611.
[69] C. Moreno-Castilla, F. Carrasco-Marín, C. Parejo-Pérez, M.V. López Ramón, Carbon 39 (2001) 869–875, https://doi.org/10.1016/S0008-6223(00)00192-5.
[70] X. Wang, Y. Song, C. Huang, F. Liang, B. Chen, Green Chem. 16 (2014) 4234–4240, https://doi.org/10.1039/C4GC00811A.
[71] Luyang Li, Feng Shen, Richard L. Smith, Xinhua Qi, Green Chem. v. 19 (2017), https://doi.org/10.1039/c6gc02443b, 76-81–2017 v.19 no.1.
[72] Y. Sun, L. Shi, H. Wang, G. Miao, L. Kong, S. Li, Y. Sun, Sustain. Energy Fuels. 3 (2019) 1163–1171, https://doi.org/10.1039/C9SE00020H.
[73] Y.I. Matatov-Meytal, M. Sheintuch, Ind. Eng. Chem. Res. 37 (1998) 309–326, https://doi.org/10.1021/ie9702439.
[74] E. Taarning, S. Saravanamurugan, M. Spangsberg Holm, J. Xiong, R.M. West, C. H. Christensen, ChemSusChem. 2 (2009) 625–627, https://doi.org/10.1002/cssc.200900099.
[75] C.H. Bartholomew, Appl. Catal. A Gen. 212 (2001) 17–60, https://doi.org/10.1016/S0926-860X(00)00843-7.
[76] L. Li, X. Collard, A. Bertrand, B.F. Sels, P.P. Pescarmona, C. Aprile, J. Catal. 314 (2014) 56–65, https://doi.org/10.1016/j.jcat.2014.03.012.